RSC Advances

PAPER

View Article Online
View Journal | View Issue

Cite this: *RSC Adv.*, 2024, **14**, 31143

High-selectivity turn-on fluorescence-based fluoride ion detection using histidine-functionalized UiO-66-NH_2†

Muh Rizal B, Mudasir and Fajar Inggit Pambudi *

Received 7th June 2024
Accepted 13th September 2024

DOI: 10.1039/d4ra04169k

rsc.li/rsc-advances

Hisditine-functionalized UiO-66-NH_2 (UiO-66-NH_2@Hst) as a novel "turn-on" fluorescent probe to detect fluoride ions has been successfully synthesized using the solvothermal method. The results showed that fluoride ion detection gave the best fluorescence response in water media and no response was observed in non-polar solvents. Detection at pH 3–10 produces a relatively similar fluorescence response and decreases quite significantly at pH 11–13. UiO-66-NH_2@Hst is very selective and stable towards fluoride ions as evidenced by the appearance of blue luminescence under UV light (λ_{365} nm) compared to other ions. A possible mechanism for detecting fluoride ions is through the formation of hydrogen bonds, which results in incremental electron transfer from organic ligands to Zr-oxo clusters. The LoD value obtained in this study was 0.013 ppm, which is smaller than the maximum concentration of fluoride ions in drinking water samples (1.5 ppm) set by the World Health Organization (WHO). Therefore, UiO-66-NH_2@Hst can be a candidate fluorescence-based sensor for fluoride ions.

Introduction

Fluoride ions are one of the critical ions that the body needs in small amounts of roughly 0.5–1.5 mg per day to strengthen tooth enamel and fend off osteoporosis.[1,2] The World Health Organization (WHO) states that there should be no more than 1.5 ppm of fluoride ions in drinking water.[3] Nevertheless, an overabundance of fluoride ions in the body can result in bone cancer, kidney disease, and fluorosis.[4] Therefore, developing methods and materials that are selective for detecting fluoride ions in drinking water samples is very important.

Selective ion electrodes,[5] ion chromatography,[6] capacitively coupled contactless conductivity detection-based capillary electrophoresis,[7] spectrophotometry,[8] ^{19}F-NMR analysis, high-performance liquid chromatography (HPLC), and mass spectroscopy (MS) are among the frequently used methods for fluoride ion analysis.[9] These methods suffer drawbacks, including complex analysis procedures, long response times, sensitivity to other ions, and high analysis costs. Fluorescence-based fluoride ion detection is a fairly efficient method because it has advantages such as simple analytical techniques, cost-efficient experiments, and high selectivity and sensitivity.[10] Additionally, it can be applied to the anion imaging of living cells.[11]

Based on the target analyte and the electronic properties of the fluorophore molecule, fluorescence intensity-based sensors are grouped into two types: namely turn-off and turn-on fluorescence.[12] Turn-off fluorescence sensors are generally more difficult to use in imaging applications because the loss of emission due to interaction with the analyte makes it difficult to distinguish or identify. In contrast, in turn-on fluorescence, observing the increase in emission from the dark state is easier than identifying the quenching process in turn-off fluorescence.[13,14] Fluorescence-based fluoride ion detection can be carried out using materials based on graphene oxide,[15] organoboron compounds,[16] organic compounds,[17–19] mesoporous silica, quantum dots, gold nanoparticles, polymers,[20] and metal–organic frameworks (MOFs).[10,21–24] Among these materials, MOFs are candidate materials that are currently being widely developed for fluoride ion detection because the crystalline nature of the framework aids in the establishment of structure–property correlation. The atomic location of the guest interaction site facilitates confirmation of the sensing mechanism. The porous nature of MOFs allows for the smooth transfer of analytes through their voids, resulting in a higher concentration of analytes in their pores and a lower limit of detection. Lastly, highly luminescent MOFs offer ultra-selectivity, ultra-sensitivity, and a quick response time.[14,25–27]

Metal–organic frameworks (MOFs) are hybrid materials or coordination polymers that are formed through coordination bonds between metal ions and organic ligands. Currently, there are many types of MOFs, but only a few show good luminescence properties, such as MOFs with lanthanide metal ions (Eu^{3+}, Tb^{3+}, Sm^{3+}, and Ce^{4+}),[14,21,28,29] aluminum-based MOFs,[30,31] and zirconium-based MOFs.[22,32,33] The Zr-based MOFs, particularly the UiO-66 family, have demonstrated significant potential for

Department of Chemistry, Faculty of Mathematics and Natural Science, Universitas Gadjah Mada, Yogyakarta, 55281, Indonesia. E-mail: fajar.inggit@ugm.ac.id

† Electronic supplementary information (ESI) available. See DOI: https://doi.org/10.1039/d4ra04169k

fluoride detection because of their strong coordination connections between the extremely stable secondary building units (SBUs) of $Zr_6O_4(OH)_4$ and benzene-1,4-dicarboxylate linkers, which result in their high porosity and sturdy structure.[24,34,35] Zhu *et al.* used UiO-66-NH_2 which has an amino group as a receptor to produce a fluorescent signal that is very sensitive and selective for fluoride ions in an aqueous solution.[10]

Attempts to increase the selectivity and sensitivity for fluoride ion detection have been reported for zirconium-based MOFs, such as by modifying UiO-66 with Tb^{3+} (ref. 21) and 3D hierarchical UiO-66-NH_2 nanoparticle/γ-AlO(OH).[23] However, research on the functionalization of UiO-66-NH_2 with certain molecules to increase its selectivity and sensitivity for fluoride ion detection is still very limited, so it remains a challenge. Therefore, we tried to functionalize the amine group on UiO-66-NH_2 with histidine to obtain UiO-66-NH_2@Hst, which shows better performance in the detection of fluoride ions. The novelty of this research is the successful functionalization of UiO-66-NH_2 with histidine *via* a one-step synthesis method with different acid modulators (acetic acid, HF, HCl, and formic acid). In this research, we have studied the effect of different types of solvent media (non-polar, aprotic polar, and protic polar solvents) on the detection of fluoride ions. The same thing also applies to the effect of pH. For the selectivity test, we tested it with more cations and anions to provide in-depth information about the level of selectivity of the material we have synthesized.

Experimental

Preparation of UiO-66-NH_2@Hst

All chemicals obtained from Sigma-Aldrich and all solvents from ACS Reagent Chemicals with a purity of >99% were used directly without further purification. UiO-66-NH_2@Hst was synthesized by modifying a previous method.[36] A total of 0.4 mmol of $ZrOCl_2 \cdot 8H_2O$ and 0.6 mmol of 2-amino-terephthalic acid ($H_2BDC\text{-}NH_2$) were dissolved in 10 mL of *N*,*N*-dimethylformamide (DMF) and sonicated for 10 minutes. After the sonication process, 0.15 mmol of histidine was added to the mixture which had previously been dissolved in 5 mL of DMF and 1 mL of acid modulator (acetic acid, formic acid, HCl, and HF 6.9 M) and then sonicated again for 5 minutes.

Next, the mixture was transferred to a Duran bottle and heated in an oven for 24 hours at a temperature of 110 °C. The solid obtained was then cooled to room temperature and centrifuged for 10 minutes at 6000 rpm. The solid product was washed three times with 15 mL of DMF and ethanol and then soaked in 20 mL of ethanol for 24 hours at room temperature. Finally, the solid was dried at a temperature of 80 °C for 24 hours to obtain a yellow powder which was UiO-66-NH_2@Hst.

Characterization

UiO-66-NH_2@Hst was characterized using X-ray diffraction (XRD, Brucker AXS D8 Advance Eco) with Cu Kα ($\lambda = 1.5418$ Å) radiation, and the patterns were collected in the 2θ range of 3–50°. Fourier transform infrared spectroscopy (FT-IR, Thermo Scientific Nicolet iS10) was also performed using pressed KBr pellets. To examine the morphology of UiO-66-NH_2@Hst, a field emission scanning electron microscope (FE-SEM, JSM-IT700HR) and transmission electron microscope (TEM, JEOL JEM-1400) were used. For the SEM analysis, the UiO-66-NH_2@Hst samples were dispersed in the SEM sample holder and coated with gold. For TEM sample preparation, the UiO-66-NH_2@Hst material was dispersed in water before being placed in a copper grid sample holder to obtain a dispersed microcrystalline representation of the sample. The calculation of the particle size of the microcrystalline samples was conducted based on the TEM image analyses. Surface area analysis was performed using a surface area analyzer (Micromeritics Gemini VII Version 5.30, Serial 2037), preceded by degassing the samples at 120 °C for 4 hours. The Brunauer–Emmett–Teller (BET) method was used to calculate specific surface areas. Adsorption peaks were recorded with a UV-vis spectrophotometer (Thermo Scientific GENESYS 150). Fluorescence intensity was measured with a spectrofluorometer (RF-6000 Shimadzu).

Fluorescence sensing experiments

To identify the MOF probes that have the best performance for fluoride ion detection, 2 mg L^{-1} of each material (UiO-66-NH_2 and UiO-66-NH_2@Hst with different acid modulators: AA, HCl, HF, and FA) was interacted with 10 mL of 1000 ppm fluoride ions. Subsequently, the mixture was sonicated for 1 minute (2 mg mL^{-1} and 1 minute are the optimum detection conditions (Fig. S1a and b ESI†)). The fluorescence intensity was measured at a wavelength of 300–600 nm with excitation at 328 nm.

The effect of the solvent medium was studied by interacting 2 mg mL^{-1} of UiO-66-NH_2@Hst (AA) with 10 mL of 1000 ppm fluoride ion solution in DI water, methanol, DMSO, THF, ethanol, ethyl acetate, acetonitrile, DMF, acetone, *n*-hexane, toluene, and dichloromethane. The mixture was sonicated for 1 minute; then the fluorescence intensity was measured at a wavelength of 300–600 nm with excitation at 328 nm.

The effect of pH on the detection of fluoride ions was studied by adjusting the pH of the fluoride ion solution using HCl and NaOH. Then, 10 mL of 1000 ppm fluoride ion solution at this pH (pH 3–13) was interacted with 2 mg mL^{-1} of UiO-66-NH_2@Hst (AA). The mixture was sonicated for 1 minute, and the fluorescence intensity was measured at a wavelength of 300–600 nm with excitation at 328 nm. For the selectivity test, 10 mL of 1000 ppm anion-cations (Cl^-, Br^-, I^-, NO_3^-, NO_2^-, SO_4^{2-}, SO_3^{2-}, HSO_4^-, $S_2O_3^{2-}$, $S_2O_5^{2-}$, $S_2O_7^{2-}$, $S_2O_8^{2-}$, BrO_3^-, PO_4^{3-}, CNS^-, Ca^{2+}, Mg^{2+}, Ba^{2+}, Hg^{2+}, Pb^{2+}, Zn^{2+}, Ni^{2+}, Cr^{3+}, and Fe^{2+}) was interacted with 2 mg mL^{-1} of UiO-66-NH_2@Hst (AA), and the luminescence phenomenon was observed under UV light at 365 nm. Anti-interference was carried out by mixing 5 mL of 1000 ppm fluoride ions and 5 mL of 1000 ppm anions–cations.

Interaction stability measurements were carried out by interacting 2 mg mL^{-1} UiO-66-NH_2@Hst (AA) with 10 mL of 1000 ppm fluoride ion solution. The mixture was sonicated for 1 minute and left for 1, 7, 15, 30, and 50 days at ambient temperature, and then the intensity was measured over that period. For the reusability test, 50 mg of UiO-66-NH_2@Hst (AA) was interacted with 10 mL of 1000 ppm fluoride ions by

sonicating the mixture for 5 minutes, and the fluorescence intensity was measured. After the interaction, the mixture was separated by centrifugation at 6000 rpm for 10 minutes and then washed with 10 mL of ethanol and DI water three times. The solid material was dried at a temperature of 80 °C for 24 hours. The dried UiO-66-NH_2@Hst (AA) was used for fluoride ion sensing again for 5 cycles. After UiO-66-NH_2@Hst (AA) was used, the solid was characterized using XRD and FTIR.

Results and discussion

Characterization of UiO-66-NH_2@Hst

The synthesis process of UiO-66-NH_2@Hst (Fig. S2 ESI†) used different acid modulators, namely acetic acid (AA), formic acid (FA), hydrogen fluoride (HF), and hydrogen chloride (HCl). This acid modulator functions to control the growth of crystal size and morphology.[37] It also acts as an acid catalyst in the reaction

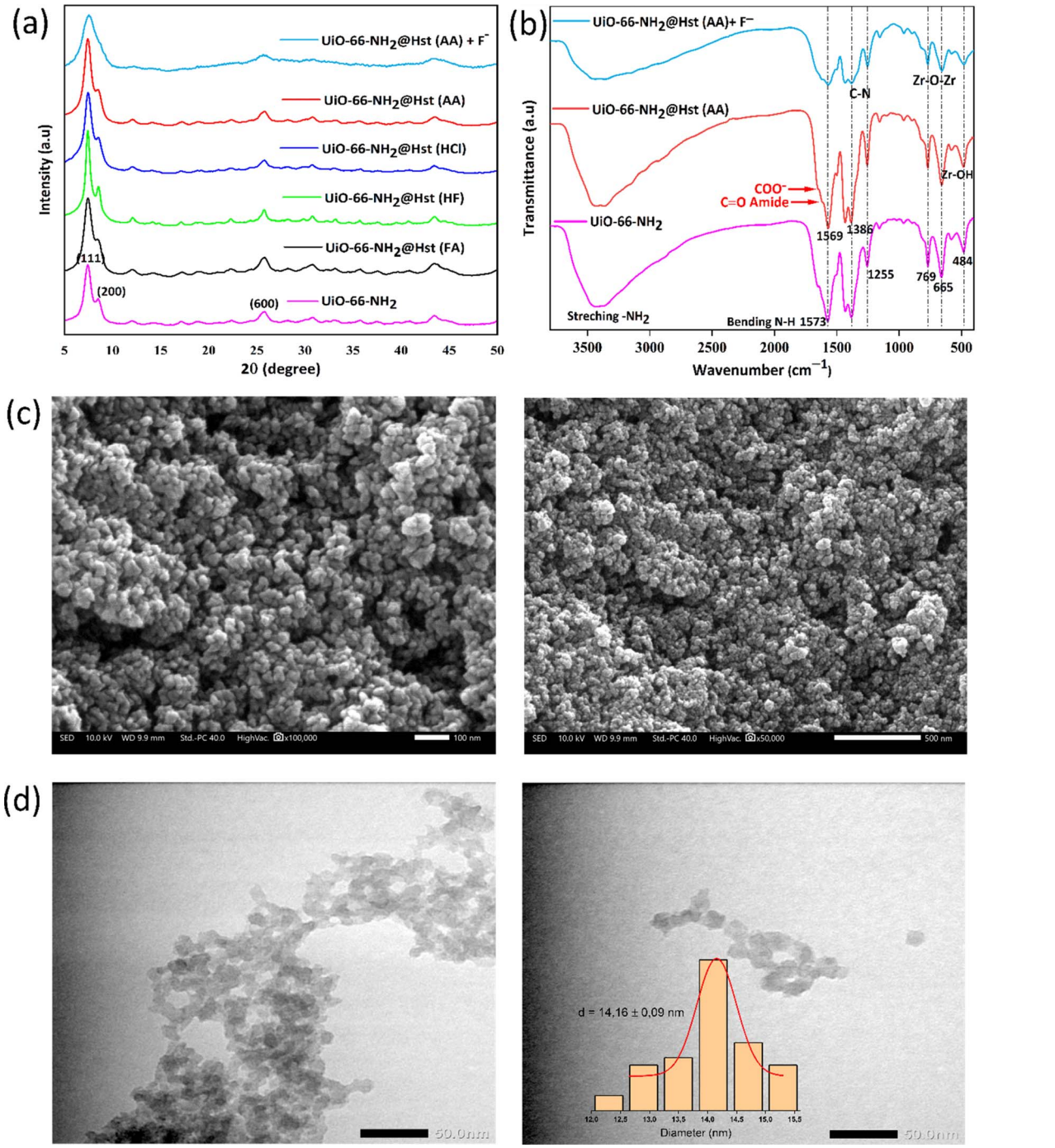

Fig. 1 XRD patterns of UiO-66-NH_2 and UiO-66-NH_2@Hst with different acid modulators (a); FT-IR spectra of UiO-66-NH_2, UiO-66-NH_2@Hst (AA) and UiO-66-NH_2@Hst (AA) in the presence of fluoride ions (b); FE-SEM images of UiO-66-NH_2@Hst (AA) with different scale bars of 100 (left) and 500 (right) nm (c); TEM images of UiO-66-NH_2@Hst (AA) with a scale bar of 50 nm on different spots and the average distribution of particle size (d).

between histidine and UiO-66-NH_2. The success of the synthesis of UiO-66-NH_2@Hst was proven by characterization using XRD and FTIR. Fig. 1a shows three main peaks appearing at 2θ around 7.46°(111), 8.52°(200), and 25.81°(600), which are the characteristic peaks of UiO-66-NH_2,[10,38,39] indicating that UiO-66-NH_2 has been successfully synthesized. After functionalization with histidine on various acid modulators, there were no peaks that were significantly different from the XRD peak of UiO-66-NH_2. This means that the functionalization of UiO-66-NH_2 with histidine did not produce a new crystal phase.[40,41]

Fig. 1b shows the FT-IR spectra of UiO-66-NH_2, UiO-66-NH_2@Hst(AA), and UiO-66-NH_2@Hst(AA) after reacting with fluoride ions. Absorption peaks at wavenumbers 484, 665, and 769 cm^{-1} are typical of stretching vibrations of Zr–OH and Zr–O–Zr. Aromatic C–N stretching appears at absorption peaks of 1255 and 1386 cm^{-1}. N–H bending vibration is found at absorption 1573 cm^{-1}. The broad peaks around 3367 and 3455 cm^{-1} are typical vibrations of the amine group (–NH_2).[10,23,42] The success of the functionalization process is indicated by the appearance of a weak absorption peak at wavenumber 1620 cm^{-1}. This is attributed to the C=O moiety of the amide functionality and a shift in N–H bending vibrations occurring from 1573 cm^{-1} to 1569 cm^{-1}.[41,43,44]

The N_2 adsorption–desorption isotherm of UiO-66-NH_2 and UiO-66-NH_2@Hst is shown in Fig. S3 ESI.† The Brunauer–Emmett–Teller (BET) surface area of UiO-66-NH_2 from the isotherm is calculated as 314.29 m^2 g^{-1}. After functionalization, the value of the BET surface area was 220.76 m^2 g^{-1}. This decrease was caused by histidine occupying space or pores on the surface of UiO-66-NH_2.[45,46] In addition, the morphology and internal structure of UiO-66-NH_2@Hst (AA) were investigated using FE-SEM (Fig. 1c) and TEM (Fig. 1d). The SEM images (Fig. 1c) indicate a consistent spherical surface shape, and its microstructure resembles interlocking particles (Fig. 1d) with a diameter of about 14 nm.

Luminescence property of UiO-66-NH_2@Hst

Turn-on fluorescence-based sensors occur due to the enhancement of a new emission peak (ON) when reacting with a specific analyte that was previously dark or had weak intensity (OFF).[47] Fig. 2a shows the result of the initial screening of UiO-66-NH_2 and UiO-66-NH_2@Hst with different acid modulators for their ability to detect fluoride ions. The results show that UiO-66-NH_2 modified with histidine has a significantly better fluoride ion detection intensity, which proves that the presence of histidine affects the material performance. In addition, UiO-66-NH_2@Hst

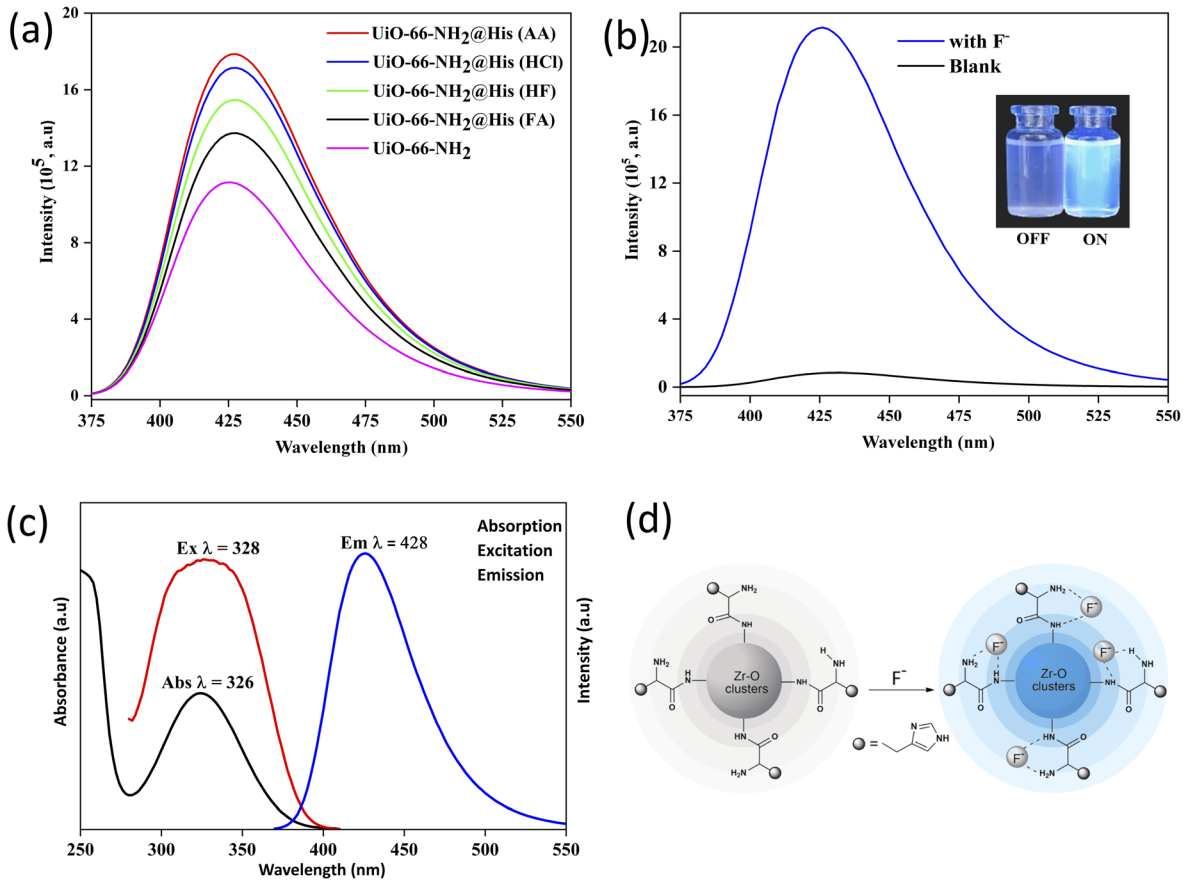

Fig. 2 Intensity fluorescence of UiO-66-NH_2@Hst with different acid modulators in the presence of fluoride ions (a); emission of UiO-66-NH_2@Hst (AA) revealing the strong change in fluorescence change after the addition of F^- (the insert shows a photograph of OFF–ON phenomena under UV light) (b); absorption, excitation, and emission spectra of UiO-66-NH_2@Hst (AA) in the presence of fluoride ions (c); and the possible schematic interaction between UiO-66-NH_2@Hst (AA) and fluoride ions (d).

with AA modulator has a detection intensity response to fluoride ions that is higher than that of UiO-66-NH_2 or other UiO-66-NH_2@Hst. This is because AA as a modulator can reduce defects in MOFs.[29] In subsequent characterization and testing, we used UiO-66-NH_2@Hst (AA) as the main material. In Fig. 2b, the fluorescence response of UiO-66-NH_2@Hst (AA) with and without the presence of fluoride ions shows significant differences in fluorescence intensity. The fluorescence response without the presence of fluoride ions has very low intensity. However, when fluoride ions are added, the intensity rises significantly at the wavelength of 428 nm.

To understand the process of fluorescence, the absorption, excitation, and emission peaks of UiO-66-NH_2@Hst were measured, as given in Fig. 2c. The absorption peak at 326 nm is the $\pi \rightarrow \pi^*$ electronic transition of the aromatic ring of the ligand.[23,48] Under 328 nm excitation, the emission peak is observed at 428 nm, which is the existence of a fluorescence process that occurs due to the transfer of charge or electrons from the π-aromatic to the Zr–O bond cluster (ligand-to-metal charge transfer).[49] The electron transfer process is proven by EPR spectroscopy, where Zr^{4+} is reduced to Zr^{3+} due to the transfer of electrons to the 4d orbital on zirconium.[29,50]

The interaction between fluoride ions and UiO-66-NH_2@Hst (AA) occurs through the formation of hydrogen bonds, as schematically illustrated in Fig. 2d. This interaction is indicated by the widening of the amine vibrational absorption peak at wavenumbers around 3367 and 3440 cm^{-1} (see Fig. 1b). This interaction is similar to those reported in some previous studies.[10,23,29] The presence of fluoride ions is predicted to increase the electron density around the organic linker that has been modified by histidine. This might increase the possibility of electron transfer from ligand to metal to give an enhanced fluorescence response, as indicated by the turn-on phenomenon. This indicates that UiO-66-NH_2@Hst is a promising candidate for the turn-on sensing of fluoride ions.

Effects of solvent media and pH

One of the key components of the sensor is the solvent medium. The degree to which the solvent affects the capacity of UiO-66-NH_2@Hst for detection is relevant to this. Different types of solvents have been tested, including *n*-hexane, acetone, toluene, and dichloromethane as non-polar solvents; water, methanol, and ethanol as protic polar solvents; and DMSO, DMF, THF, ethyl acetate, and acetonitrile as aprotic polar solvents. In Fig. 3a, the non-polar solvent detection medium (*n*-hexane, toluene, acetone, and dichloromethane) indicates no fluorescence intensity. This is due to the very low solubility of NaF as a source of fluoride ions in these solvents, so no fluoride ions are present in the solvent. These solvents also cannot disperse UiO-66-NH_2@Hst (AA), resulting in no interaction between UiO-66-NH_2@Hst (AA) and fluoride ions in the medium. This is further proven by the absence of blue photoluminescence under UV light at 365 nm (Fig. S4, ESI†). In the solvent media of methanol, DMSO, THF, ethanol, ethyl acetate, acetonitrile, and DMF, a significant reduction in fluorescence intensity (quenching effect) is observed compared to water media. The different degrees of quenching impacts may be attributed to the diverse interaction forces between UiO-66-NH_2@hst and the solvents used, further influencing the electron transfer process.[51,52] For the next detection process, we used water as the medium because it has the best fluorescence response and can disperse UiO-66-NH_2@Hst (AA) and dissolve NaF as the source of fluoride ions.

Environmental samples or beverages containing fluoride ions generally have different pH. Therefore, evaluating the effect of pH on fluoride ion detection is very important. Fig. 3b shows the effect of pH on the fluorescence intensity response. In Fig. 3b, it can be seen that pH does not shift the emission peak of fluoride ion detection, where the emission peak remains at 428 nm.[21] The fluorescence intensity response for fluoride ion detection is essentially the same at acidic and alkaline pH (3–10), indicating that the UiO-66-NH_2@Hst(AA) material is still stable in this pH range.[10] However, there is a sharp drop in

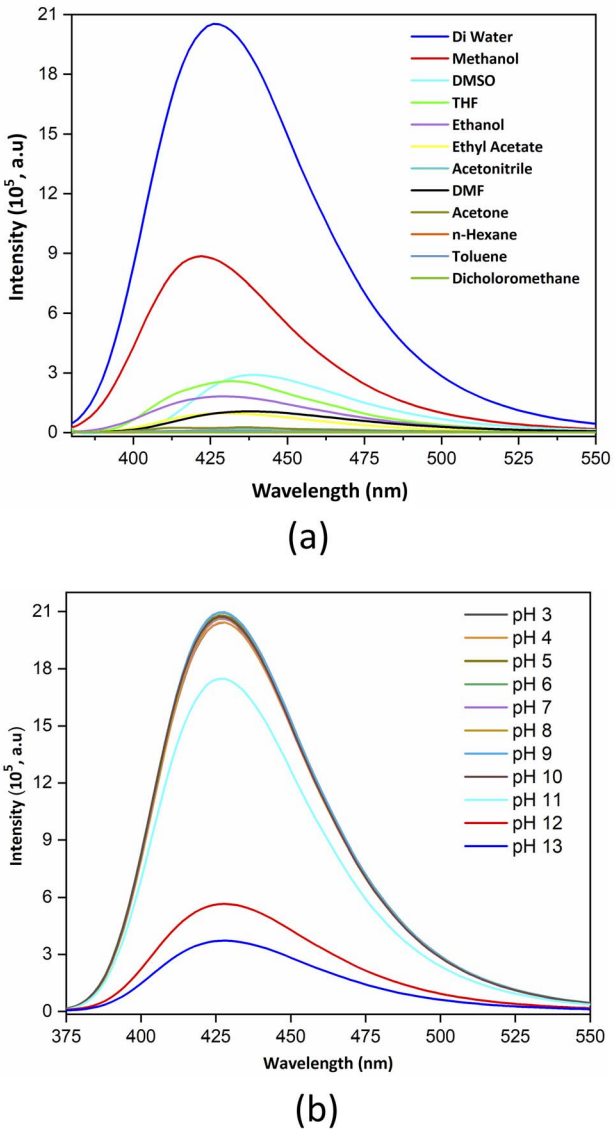

Fig. 3 The intensity of fluoride ion detection in various solvent media (a); and the intensity of fluoride ion detection at various pH (3–13) (b) using UiO-66-NH_2@Hst (AA).

fluorescence intensity at extreme pH (pH 11–13), which can be attributed to several causes. First, under higher alkaline conditions, the concentration of hydroxide ions in the solution becomes very abundant, thus becoming a barrier for fluoride ions to interact with the active sites of UiO-66-NH_2@Hst(AA). Second, it is caused by deprotonation of the amino group on histidine in the UiO-66-NH_2 framework,[53] where histidine will have a negative charge if the pH of the solution is greater than its pKa_3 value (pKa_3 = 9.17). The change in charge on histidine causes the fluoride ion, which has also a negative charge, to have difficulty interacting with the UiO-66-NH_2@Hst. Third, it might be caused by damage to the structure or framework of UiO-66-NH_2@Hst(AA), so that the abundance of active sites decreases. Zheng *et al.* stated that when the pH of fluoride ion detection is greater than 10, damage will occur to the Tb^{3+}@Zr-MOF framework, thereby hampering the detection process.[21] Damage to the MOF material framework is caused by hydroxyl ions which may break the bonds between the ligand and the Zr cluster.[54] This bond breaking is due to the strong affinity between the high-valence Zr^{4+} ion and the hydroxyl anion.[29]

Selectivity and anti-interference

Selectivity is the ability of a material to respond to only one analyte. The selectivity test aims to see the level of selectivity of UiO-66-NH_2@Hst towards fluoride ions, while the anti-interference test aims to determine how much influence the interference anion or cation has on the target anion. This test is important because the real sample contains many other anions and cations that can be a nuisance during testing. A good material is a material that only responds to one analyte even though there are many interfering ions in the solution. In the selectivity and anti-interference tests, anions (F^-, Cl^-, Br^-, I^-, NO_3^-, NO_2^-, SO_4^{2-}, SO_3^{2-}, HSO_4^-, $S_2O_3^{2-}$, $S_2O_5^{2-}$, $S_2O_7^{2-}$, $S_2O_8^{2-}$, BrO_3^-, PO_4^{3-}, CNS^-) and cations (Ca^{2+}, Mg^{2+}, Ba^{2+}, Hg^{2+}, Pb^{2+}, Zn^{2+}, Ni^{2+}, Cr^{3+}, Fe^{2+}) are used, as shown in Fig. 4. In Fig. 4a, it can be seen that UiO-66-NH_2@Hst (AA) shows high selectivity towards fluoride ions, as evidenced by the highest peak detection fluorescence intensity compared to the anions–cations tested. This is also supported by the appearance of bright blue photoluminescence under UV light at 365 nm

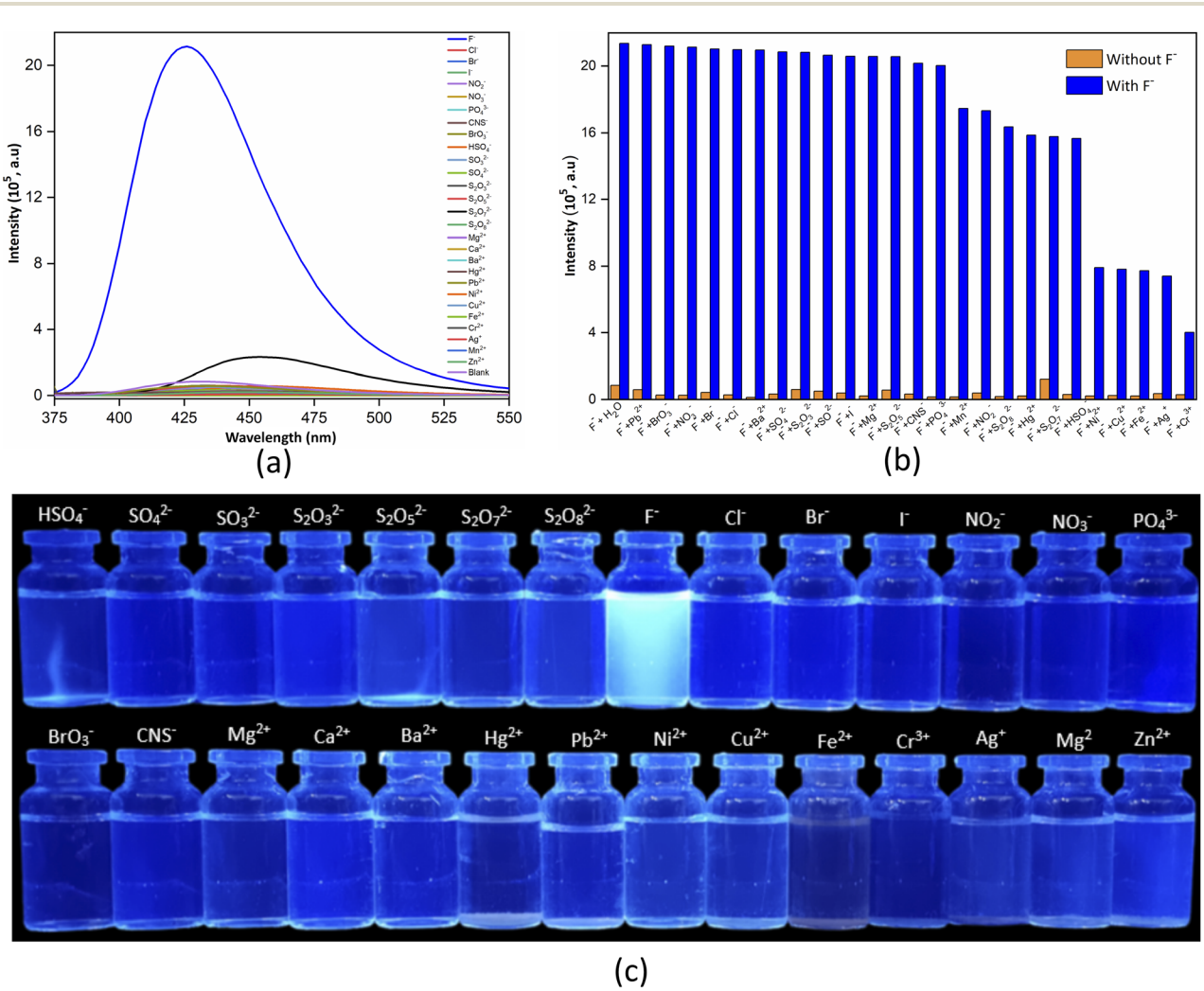

Fig. 4 Selectivity test of UiO-66-NH_2@Hst (AA) in 10 mL of 1000 ppm anions–cations (a); the anti-interference test of fluoride ions and anions–cations with a ratio of 1 : 1 (v/v) (b); and the luminescence of various anions–cations under UV light at 365 nm.

(Fig. 4c). The fluoride ion has a very high electronegativity and a small radius (1.33 Å),[55,56] so it very easily enters the UiO-66-NH_2@Hst (AA) framework to interact with the active site of UiO-66-NH_2@Hst (AA).

To check the potential of UiO-66-NH_2@Hst (AA) as a fluorogenic sensor for fluoride detection, the fluorescence response of a UiO-66-NH_2@Hst (AA) suspension in the presence of various anions–cations was investigated. Due to the complicated environment of the aqueous solution, the influence of the other anions–cations on the sensing of fluoride ions should also be evaluated to assess the possibility of practical application. The anion–cation interference test on fluoride ions is shown in Fig. 4b. Based on Fig. 4b, it can be seen that the anions–cations tested without the presence of fluoride ions did not give a fluorescence intensity response (the fluorescence intensity was relatively weak). After the addition of fluoride ions, there was a significant increase in the detection fluorescence intensity. This proves that the increase in fluorescence intensity is caused by the presence of fluoride ions in the solution. Ni^{2+}, Cu^{2+}, Fe^{2+}, Ag^{+}, and Cr^{3+} cations exert a stronger influence on the fluorescence intensity. This can be caused by the metal cation forming a chelate with the amino group on UiO-66-NH_2@Hst (AA), thereby blocking the interaction between the fluoride ion and UiO-66-NH_2@Hst (AA). Based on the selectivity and anti-interference tests, it can be concluded that the UiO-66-NH_2@Hst (AA) material is highly selective towards fluoride ions alone and UiO-66-NH_2@Hst (AA) shows good anti-interference properties, which are vital for fluorescent probes.

Linearity and limit of detection (LoD)

Linearity refers to the degree to which a material can respond to a particular analyte proportionally and consistently as the analyte concentration increases. In Fig. 5a, it can be seen that the increase in fluoride ion concentration is linear with the

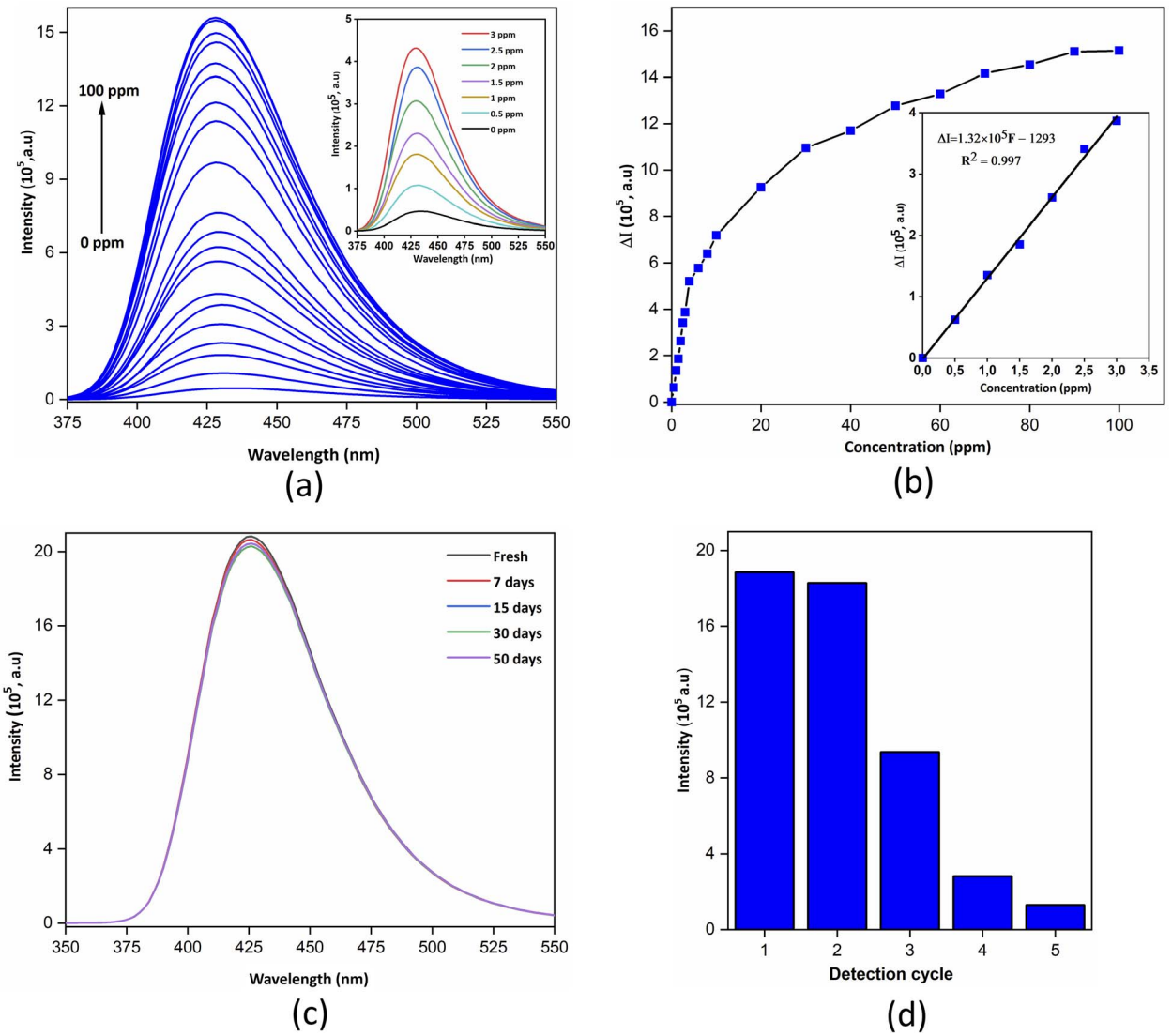

Fig. 5 The influence of fluoride ion concentration on the fluorescence intensity (a); linearity curve in the range of 0–100 ppm of fluoride ions (insert image: 0–3 ppm) (b); the stability test of the interaction between UiO-66-NH_2@Hst (AA) and fluoride ions up to 50 days (c); and the reusability of UiO-66-NH_2@Hst (AA) with the ratio of 50 mg to 10 mL of 1000 ppm fluoride ions (d).

Table 1 Comparison of the detection limit of UiO-66-NH_2@Hst (AA) with other MOF probes

MOF probes	Detection type	LoD (ppm)	Number of ions tested	Ref.
Pyrene-tagged UiO-66-NH_2	Turn-on	0.015	9	57
FS@UiO-66	Turn-on	0.084	8	22
Tb^{3+}@Zr-MOFs	Turn-on	0.35	11	21
UiO-66-NH_2	Turn-on	0.299	15	10
Co-MOFs	Turn-on	0.24	10	58
UiO-66-NH_2-γ-AlO(OH)	Turn-on	0.015	13	23
EuTPTC-NH_2	Ratiometric	0.213	10	59
UiO-66-NH_2-FITC	Colorimetric and turn-on	0.065	10	35
UiO-66-NH_2@Hst (AA)	Turn-on	0.013	28	This work

resulting fluorescence intensity (turn-on fluorescence). This is caused by the increased electron transfer of fluoride ions to the active sites of UiO-66-NH_2@Hst (AA). The linearity plot shows the relationship between ($\Delta\iota$) and concentration (ppm). Here, $\Delta\iota$ is the result of subtracting the fluorescence intensity of the analyte in the sample (ι) from the blank intensity (ι_o) ($\Delta\iota = \iota - \iota_o$).[48] Linearity is measured in the range of 0–100 ppm, but the best linearity is in the range of 0–3 ppm. Based on the linearity plot in Fig. 5b, the equation $\Delta\iota = 1.32 \times 10^5$ F − 1293 and the correlation coefficient ($R^2 = 0.997$) are obtained. Based on the value of the correlation coefficient, which is close to one, it can be said that the increase in fluoride ion concentration is proportional to the resulting fluorescence intensity. Therefore, the line equation obtained has a high level of accuracy and can be used for determining the limit of detection (LoD) and limit of quantification (LoQ). LoD is the lowest concentration limit of an analyte that can be detected, while LoQ is the lowest concentration of an analyte that can be measured quantitatively. The LoD and LoQ values of fluoride ion detection were obtained from the equations LoD = $3\sigma/s$ and LoQ = $10\sigma/s$, where σ is the standard deviation of 10 blank measurements and s is the slope (1.32×10^5) of the linear equation. The LoD value obtained is 0.013 ppm and LoQ is 0.045 ppm, where the value obtained is smaller than in previous research (see Table 1). According to the World Health Organization (WHO), the maximum limit of fluoride ions in drinking water is 1.5 ppm, and the LoD value obtained is smaller than the WHO provisions.[3] It can be concluded that UiO-66-NH_2@Hst (AA) can be a candidate for a fluoride ion sensor based on turn-on fluorescence.

Stability and reusability

The stability test aims to determine how long the interaction between the fluoride ions and the active sites of UiO-66-NH_2@Hst (AA) remains stable. In Fig. 5c, it can be seen that up to 50 days, the fluorescence intensity remains relatively the same. This stability is because the fluoride ion can form hydrogen bonds simultaneously with the amide and amino groups on UiO-66-NH_2@Hst(AA). Reusability is the ability of a material to provide the same response when used repeatedly. The purpose of reusability is to determine to what extent UiO-66-NH_2@Hst (AA) can be reused. Fig. 5d shows the result of five cycles of repeated use of UiO-66-NH_2@Hst (AA) for fluoride ion detection. The reusability test results show that using UiO-66-NH_2@Hst (AA) twice gives a relatively similar intensity response.

However, the intensity decreased quite significantly when the UiO-66-NH_2@Hst (AA) material was used 3–5 times. This might be caused by a collapse in the material structure,[60] thereby reducing the degree of crystallinity, as shown in Fig. 1a (UiO-66-NH_2@Hst (AA) + F^-). The collapse of UiO-66-NH_2@Hst (AA) can reduce the active sites, which play an important role in the detection of fluoride ions. This might also occur due to repeated washing with ethanol before UiO-66-NH_2@Hst (AA) is reused repeatedly. The decrease in mass of UiO-66-NH_2@Hst (AA) could also be the reason for the decrease in fluorescence intensity when reused.

Conclusions

In summary, we have successfully functionalized UiO-66-NH_2 with histidine (UiO-66-NH_2@Hst) as a novel "turn-on" fluorescent probe to detect fluoride ions. In various detection media that have been evaluated, water is the best detection medium. This is because of its good ability to disperse UiO-66-NH_2@Hst (AA). UiO-66-NH_2@Hst (AA) has good stability at pH 3–10, as evidenced by a constant fluorescence response. UiO-66-NH_2@Hst (AA) has high selectivity towards fluoride ions compared to the anions tested and shows good anti-interference. The LoD value obtained is 0.013 ppm, which is lower than the maximum limit for fluoride ions in drinking water (1.5 ppm). Therefore, UiO-66-NH_2@Hst (AA) could be a candidate for a turn-on fluorescence-based sensor for fluoride ions.

Data availability

The data supporting this article have been included as part of the ESI.†

Author contributions

The author (Muh Rizal B) confirms the responsibility for the following: synthesis of compounds, characterization, investigation, data curation, methodology, writing – original draft and writing – review & editing. The author (Mudasir) confirms the

responsibility for the following: supervision, conceptualization, validation, and writing – review & editing. The author (Fajar Inggit Pambudi) confirms the responsibility for the following: Supervision, conceptualization, validation, resources, writing – review & editing.

Conflicts of interest

There are no conflicts to declare.

References

1 S. Swami, A. Agarwala, B. Malik and R. Shrivastava, *J. Chem. Sci.*, 2016, **128**, 1451–1457.
2 H. Liu, Y. Gao, L. Sun, M. Li, B. Li and D. Sun, *Int. J. Hyg. Environ. Health*, 2014, **217**, 413–420.
3 World Health Organization, *Guidelines for Drinking-Water Quality*, 4th edition, incorporating the 1st addendum, 2017, p. 371.
4 Q. Li, Y. Wu, Y. Liu, L. Shangguan, B. Shi and H. Zhu, *Org. Lett.*, 2020, **22**, 6662–6666.
5 M. Ponikvar, V. Stibilj and B. Žemva, *Food Chem.*, 2007, **103**, 369–374.
6 A. Szmagara and A. Krzyszczak, *J. Geochem. Explor.*, 2019, **202**, 27–34.
7 I. C. Guimarães, C. C. Rezende, J. A. F. da Silva and D. P. de Jesus, *Talanta*, 2009, **78**, 1436–1439.
8 T. L. Marques and N. M. M. Coelho, *Talanta*, 2013, **105**, 69–74.
9 X. Liu, X. Liu, Y. Shen and B. Gu, *ACS Omega*, 2020, **5**, 21684–21688.
10 H. Zhu, J. Huang, Q. Zhou, Z. Lv, C. Li and G. Hu, *J. Lumin.*, 2019, **208**, 67–74.
11 Y. Liu, Y. Zhou, H. Li, J. Gao, M. Yang, Z. Yuan and X. Li, *ACS Omega*, 2022, **7**, 34317–34325.
12 F. Y. Yi, D. Chen, M. K. Wu, L. Han and H. L. Jiang, *Chempluschem*, 2016, **81**, 675–690.
13 A. Karmakar, P. Samanta, S. Dutta and S. K. Ghosh, *Chem. - Asian J.*, 2019, **14**, 4506–4519.
14 T. K. Pal, *Mater. Chem. Front.*, 2022, **7**, 405–441.
15 C. Wang, S. Yang, M. Yi, C. Liu, Y. Wang, J. Li, Y. Li and R. Yang, *ACS Appl. Mater. Interfaces*, 2014, **6**, 9768–9775.
16 C. R. Wade, A. E. J. Broomsgrove, S. Aldridge and F. P. Gabbaï, *Chem. Rev.*, 2010, **110**, 3958–3984.
17 J. Cho, I. Kim, J. H. Moon, H. Singh, H. S. Jung, J. S. Kim, J. Y. Lee and S. Kim, *Dyes Pigm.*, 2016, **132**, 248–254.
18 X. Chen, Y. C. Liu, J. Bai, H. Fang, F. Y. Wu and Q. Xiao, *Dyes Pigm.*, 2021, **190**, 109347, DOI: **10.1016/j.dyepig.2021.109347**.
19 D. Mohanasundaram, G. G. Vinoth Kumar, S. K. Kumar, B. Maddiboyina, R. P. Raja, J. Rajesh and G. Sivaraman, *J. Mol. Liq.*, 2020, **317**, 113913, DOI: **10.1016/j.molliq.2020.113913**.
20 Y. Zhou, J. F. Zhang and J. Yoon, *Chem. Rev.*, 2014, **114**, 5511–5571.
21 H. Y. Zheng, X. Lian, S. J. Qin and B. Yan, *ACS Omega*, 2018, **3**, 12513–12519.
22 X. Zhao, Y. Wang, X. Hao and W. Liu, *Appl. Surf. Sci.*, 2017, **402**, 129–135.
23 C. Wang, Y. Lyu, J. Li, L. Li, T. Li, J. Yang, N. Xing and X. Zhang, *ACS Appl. Nano Mater.*, 2022, **5**, 3201–3212.
24 F. Ahmadijokani, H. Molavi, M. Rezakazemi, T. M. Aminabhavi and M. Arjmand, *Coord. Chem. Rev.*, 2021, **445**, 214037, DOI: **10.1016/j.ccr.2021.214037**.
25 S. Kamal, M. Khalid, M. S. Khan and M. Shahid, *Coord. Chem. Rev.*, 2023, **474**, 214859, DOI: **10.1016/j.ccr.2022.214859**.
26 Y. Zhu, L. Zhu, W. Song and C. Deng, *Inorg. Chem. Commun.*, 2023, **145**, 110917, DOI: **10.1016/j.inoche.2023.110917**.
27 J. Li, M. Liu, J. Li and X. Liu, *Talanta*, 2023, **259**, 124521, DOI: **10.1016/j.talanta.2023.124521**.
28 H. Che, Y. Li, S. Zhang, W. Chen, X. Tian, C. Yang, L. Lu, Z. Zhou and Y. Nie, *Sens. Actuators, B*, 2020, **324**, 128641.
29 M. H. Hassan and S. Andreescu, *Inorg. Chem.*, 2023, **62**, 20970–20979.
30 F. M. Hinterholzinger, B. Rühle, S. Wuttke, K. Karaghiosoff and T. Bein, *Sci. Rep.*, 2013, **3**, 2562, DOI: **10.1038/srep02562**.
31 Y. Sun, X. Xu, Y. Zhao, H. Tan, Y. Li and J. Du, *Talanta*, 2020, **209**, 120582, DOI: **10.1016/j.talanta.2019.120582**.
32 W. Fan, X. Wang, B. Xu, Y. Wang, D. Liu, M. Zhang, Y. Shang, F. Dai, L. Zhang and D. Sun, *J. Mater. Chem. A*, 2018, **6**, 24486–24495.
33 S. Mandal, S. Natarajan, P. Mani and A. Pankajakshan, *Adv. Funct. Mater.*, 2021, **31**(4), 2006291, DOI: **10.1002/adfm.202006291**.
34 Z. Yue, L. Feng and W. Feng, *Opt. Fiber Technol.*, 2022, **70**, 102885, DOI: **10.1016/j.yofte.2022.102885**.
35 Q. Li, H. Chen, S. You, Z. Lin, Z. Chen, F. Huang and B. Qiu, *Microchem. J.*, 2023, **186**, 108318.
36 F. Aghili, A. A. Ghoreyshi, A. Rahimpour and B. Van Der Bruggen, *Ind. Eng. Chem. Res.*, 2020, **59**, 7825–7838.
37 W. Morris, S. Wang, D. Cho, E. Auyeung, P. Li, O. K. Farha and C. A. Mirkin, *ACS Appl. Mater. Interfaces*, 2017, **39**, 33413–33418.
38 S. Subudhi, S. Mansingh, S. P. Tripathy, A. Mohanty, P. Mohapatra, D. Rath and K. Parida, *Catal. Sci. Technol.*, 2019, **9**, 6585–6597.
39 M. J. Katz, Z. J. Brown, Y. J. Colón, P. W. Siu, K. A. Scheidt, R. Q. Snurr, J. T. Hupp and O. K. Farha, *Chem. Commun*, 2013, **49**, 9449–9451.
40 S. J. Garibay and S. M. Cohen, *Chem. Commun*, 2010, **46**, 7700–7702.
41 S. Tripathi, B. Sreenivasulu, A. Suresh, C. V. S. B. Rao and N. Sivaraman, *RSC Adv.*, 2020, **10**, 14650–14661.
42 P. Zhu, H. Cao, H. Yang, M. Geng, S. Qin, L. Tan, X. Gao and C. Wang, *Appl. Surf. Sci.*, 2024, **652**, 159348, DOI: **10.1016/j.apsusc.2024.159348**.
43 Z. Wang, Z. Lv, A. Guo, G. Hu, J. Liu and J. Huang, *Sens. Actuators Rep.*, 2022, **4**, 100120, DOI: **10.1016/j.snr.2022.100120**.
44 L. Ghasempour and S. Asghari, *J. Mol. Struct.*, 2024, **1300**, 137172, DOI: **10.1016/j.molstruc.2023.137172**.

45 Z. Li, X. Zhang, Y. Luo, Q. Li, Y. Qin, G. Wang, S. Yang and Z. Liu, *Chem. Phys. Lett.*, 2023, **830**, 140825, DOI: 10.1016/j.cplett.2023.140825.
46 K. F. Alshammari, A. Subaihi, A. Alharbi, M. A. Khalil and A. Shahat, *J. Mol. Liq.*, 2023, **389**, 122787, DOI: 10.1016/j.molliq.2023.122787.
47 C. Jia, T. He and G. M. Wang, *Coord. Chem. Rev.*, 2023, **476**, 214930, DOI: 10.1016/j.ccr.2022.214930.
48 J. Yang, Y. Dai, X. Zhu, Z. Wang, Y. Li, Q. Zhuang, J. Shi and J. Gu, *J. Mater. Chem. A*, 2015, **3**, 7445–7452.
49 L. Shen, R. Liang, M. Luo, F. Jing and L. Wu, *Phys. Chem. Chem. Phys.*, 2015, **17**, 117–121.
50 D. Sun, Y. Fu, W. Liu, L. Ye, D. Wang, L. Yang, X. Fu and Z. Li, *Eur. J. Chem.*, 2013, **19**, 14279–14285.
51 D. Tian, Y. Li, R. Y. Chen, Z. Chang, G. Y. Wang and X. H. Bu, *J. Mater. Chem. A*, 2014, **2**, 1465–1470.
52 L. Yang, Y. L. Liu, C. G. Liu, Y. Fu and F. Ye, *RSC Adv.*, 2020, **10**, 19149–19156.
53 M. K. Bera, L. Behera and S. Mohapatra, *Colloids Surf., A*, 2021, **624**, 126792.
54 M. H. Hassan, A. B. Soliman, W. A. Elmehelmey, A. A. Abugable, S. G. Karakalos, M. Elbahri, A. Hassanien and M. H. Alkordi, *Chem. Commun.*, 2019, **55**, 31–34.
55 H. Qiu, M. Ye, M. D. Zhang, X. Zhang, Y. Zhao and J. Yu, *ACS ES&T Engineering*, 2021, **1**, 46–54.
56 Y. Zhang and L. Zhang, *J. Hazard. Mater.*, 2021, **418**, 126271.
57 R. Dalapati and S. Biswas, *Sens. Actuators, B*, 2017, **239**, 759–767.
58 M. Alhaddad and S. M. El-Sheikh, *ACS Omega*, 2021, **6**, 15182–15191.
59 K. Yu, Q. Wang, W. Xiang, Z. Li, Y. He and D. Zhao, *Inorg. Chem.*, 2022, **61**, 13627–13636.
60 L. Guo, Y. Liu, F. Qu, Z. Liu, R. Kong, G. Chen, W. Fan and L. Xia, *Microchim. Acta*, 2019, **186**, 740.